

Electronic Supporting Information

An Asymmetric Pt Diimine Acetylide Complex Providing Unique Luminescent Multinuclear Sandwich Complexes with Cu Salts

Shinnosuke Horiuchi,* Hirotaka Hiroiwa, Eri Sakuda, Yasuhiro Arikawa, and Keisuke Umakoshi*

Division of Chemistry and Materials Science, Graduate School of Engineering, Nagasaki University
Bunkyo-machi, Nagasaki, 852-8521 (Japan)

E-mail: shoriuchi@nagasaki-u.ac.jp, kumks@nagasaki-u.ac.jp

Contents

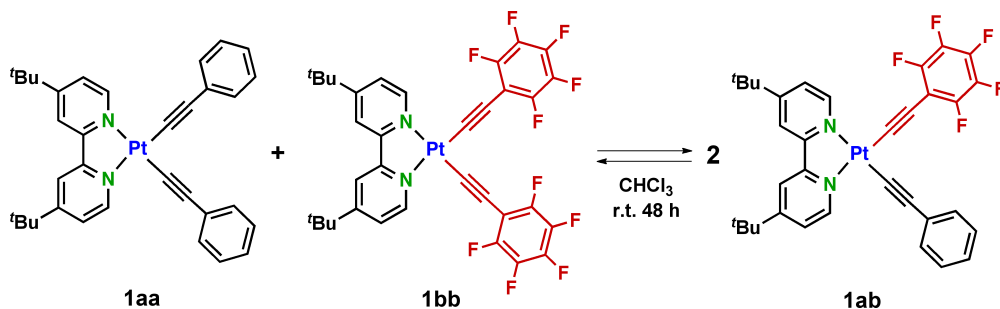
- Materials and Instrumentations
- Preparation of complexes (Figures. S1–S5)
- X-ray crystallographic analysis (Figures. S6–S7, Tables S1–S3)
- Photophysical properties (Figure S8–S10)
- Computational studies (Figures S11–S13, Tables S4–S8)

Materials and Instrumentations

The NMR spectra were obtained at 300 MHz with a Varian Gemini 300, 400 MHz with JEOL JNM-AL400 and 500 MHz with Varian NMR System 500PS spectrometer. The chemical shift values reported here with respect to an internal standard (TMS: $\delta = 0$ ppm) for ^1H NMR and an external standard (C_6F_6 : $\delta = -163.9$ ppm) for ^{19}F NMR spectroscopies. UV/Vis spectra were recorded on a Jasco V-560 spectrophotometer. Corrected emission spectra were obtained by using a Jasco FP-6500 spectrofluorometer. Lifetime measurements were conducted by using a streak camera (Hamamatsu C4334) as a detector and the third-harmonic generation of an Nd:YAG Laser (Continuum Minilite). Emission quantum yields were determined by using a Hamamatsu Photonic Absolute PL Quantum Yield Measurement System C9920-02. Temperature-dependent emission spectra were recorded by PMA-12 Photonic multichannel analyzer C10027-02. Solvents and reagents were used as purchased. Unless otherwise noted, all reactions were performed under air. Symmetric Pt complexes **1aa** and **1bb** were prepared according to established methods.^{1,2}

Preparation of complexes

Synthesis of Pt complex **1ab**



Reaction procedure: A mixture of Pt complex **1aa** (28.0 mg, 42.0 μmol) and **1bb** (35.0 mg, 42.0 μmol) in CHCl_3 (20 ml) were stirred at room temperature for 48 h. When the solution was concentrated to dryness, asymmetric Pt complex **1ab** was obtained as a statistical mixture of **1aa**, **1ab** and **1bb**. After purification of the mixture through a silica-gel column chromatography (elute: CH_2Cl_2), Pt complex **1ab** was isolated as a yellow solid (27.3 mg, 36.1 μmol , 43%).

Physical data of **1ab:** ^1H NMR (500 MHz, CDCl_3 , TMS: $\delta = 0$ ppm): $\delta = 9.69$ (d, $J = 8.0$ Hz, 1H), 9.65 (d, $J = 8.0$ Hz, 1H), 7.97 (s, 2H), 7.59 (d, $J = 8.0$ Hz, 2H), 7.53 (d, $J = 8.0$ Hz, 2H), 7.26 (t, $J = 8.0$ Hz, 2H), 7.15 (t, $J = 8.0$ Hz, 1H), 1.45 (s, 9H), 1.44 (s, 9H); ^{19}F NMR (470 MHz, CDCl_3 , C_6F_6 : $\delta = -163.9$ ppm): $\delta = -140.6$ (ddd, $J = 23, 6, \text{ and } 2$ Hz, 2F), -162.0 (t, $J = 23$ Hz, 1F), -166.7 (ddt, $J = 23, 6, \text{ and } 2$ Hz, 2F); Anal. Calcd for $\text{C}_{34}\text{H}_{29}\text{F}_5\text{N}_2\text{Pt} \cdot 0.3\text{CH}_2\text{Cl}_2$: C, 52.74; H, 3.82; N, 3.59. Found: C, 52.72; H, 4.04; N, 3.70; FAB-MS m/z calcd for $[\text{M}]^+$: 755.7, found 756.

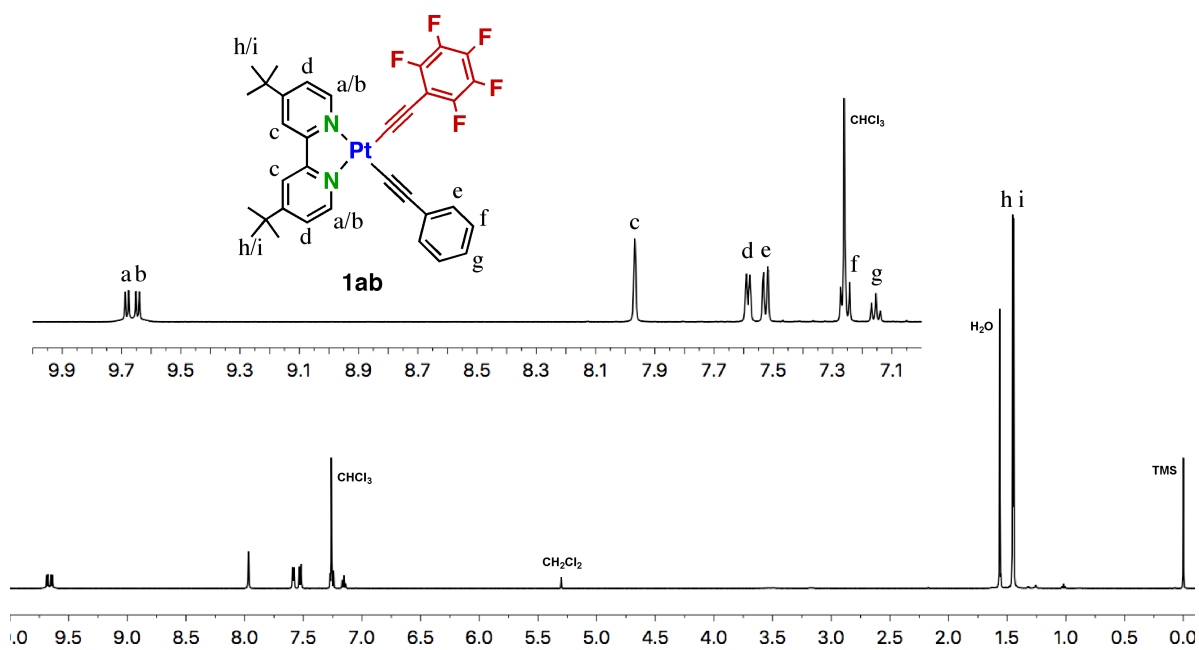


Fig. S1 ¹H NMR spectrum (500 MHz, CDCl₃, TMS) of **1ab**.

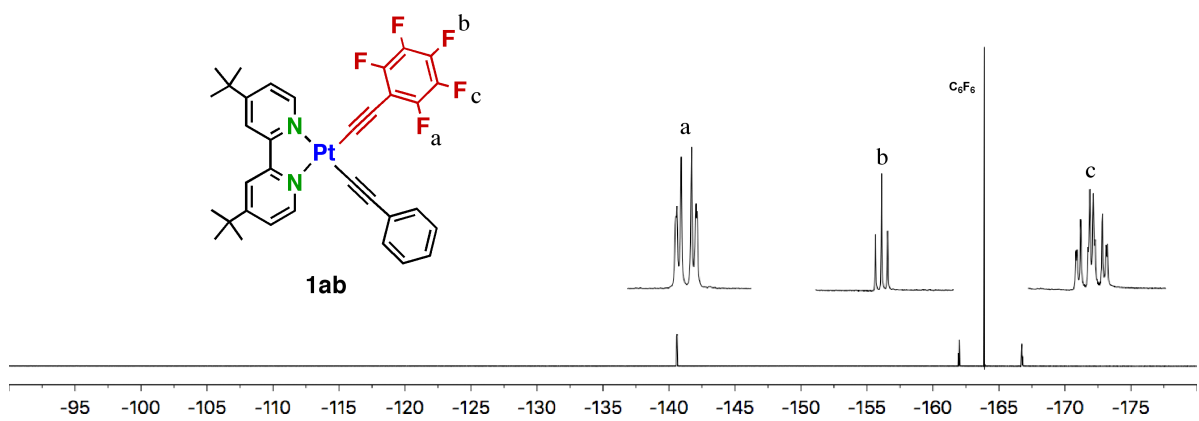


Fig. S2 ¹⁹F NMR spectrum (470 MHz, CDCl₃, C₆F₆) of **1ab**.

¹H NMR spectral variations of the acetylide ligand exchange reaction.

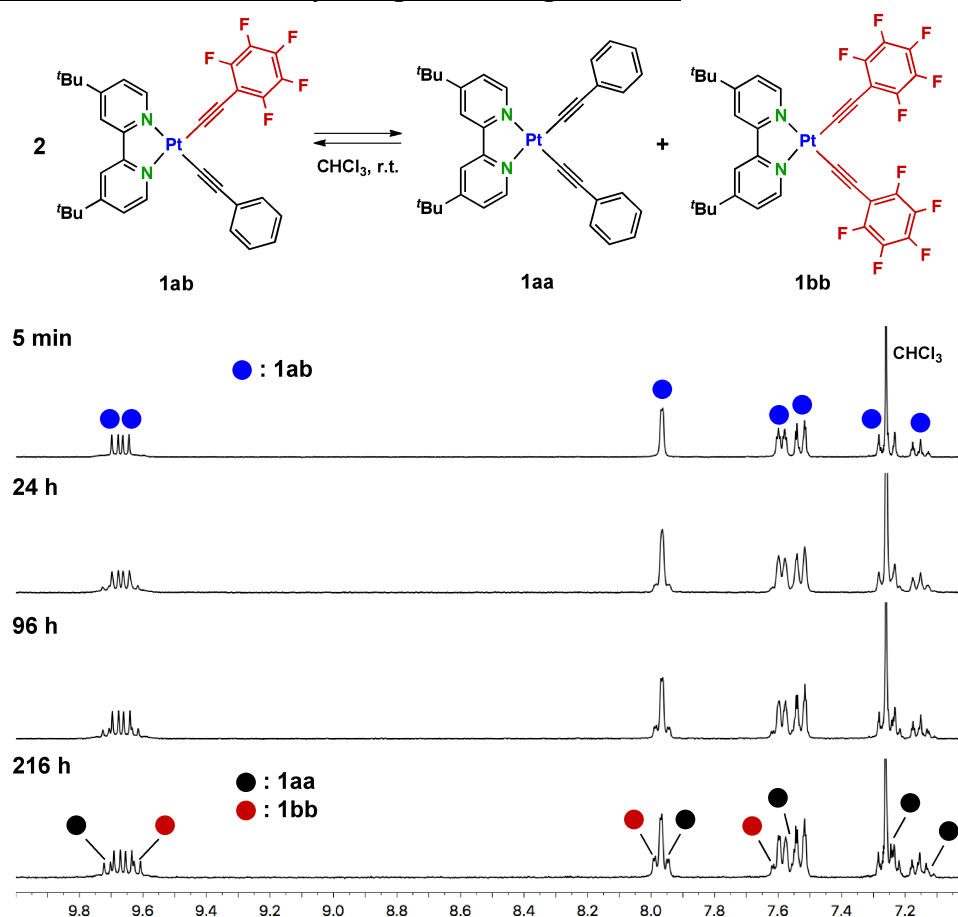


Fig. S3 ^1H NMR spectral variations (3.3 mM in CDCl_3 , r.t.) of the intermolecular ligand exchange reaction (disproportionation) of **1ab**, giving symmetric Pt complexes **1aa** and **1bb**.

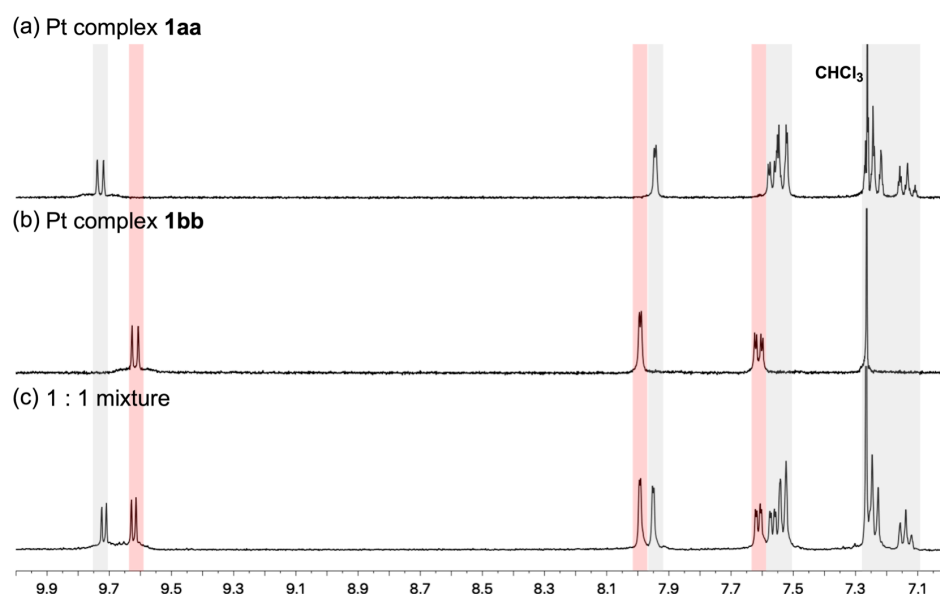
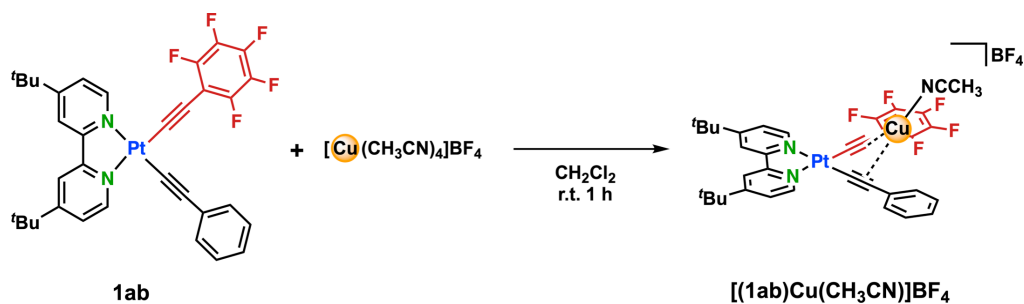


Fig. S4 ^1H NMR spectra (300 MHz, CDCl_3 , r.t.) of (a) Pt complex **1aa**, (b) Pt complex **1bb**, and (c) 1:1 mixture of **1aa** and **1bb**. The signals at around 9.65 ppm slightly shifted in the mixture, implying a reversible dimer formation in solution.

Synthesis of Pt complex [(1ab)Cu(CH₃CN)]BF₄



Reaction procedure: Pt complex **1ab** (33.7 mg, 44.6 μmol) and $[\text{Cu}(\text{CH}_3\text{CN})_4]\text{BF}_4$ (14.0 mg, 44.5 μmol) in CHCl_3 (20 ml) were stirred at room temperature under Ar atmosphere for 1 h. Addition of diethyl ether into the reaction mixture afforded the copper adduct $[(\mathbf{1ab})\text{Cu}(\text{CH}_3\text{CN})]\text{BF}_4$ as a yellow precipitate. After the solid was collected, washed with diethyl ether, and dried in vacuo, PtCu complex $[(\mathbf{1ab})\text{Cu}(\text{CH}_3\text{CN})]\text{BF}_4$ was isolated (40.1 mg, 42.3 μmol , 94%).

Physical data of $[(\mathbf{1ab})\text{Cu}(\text{CH}_3\text{CN})]\text{BF}_4$: ^1H NMR (300 MHz, acetone- d_6): δ = 9.15 (d, J = 8.0 Hz, 1H), 9.12 (d, J = 8.0 Hz, 1H), 8.76 (s, 2H), 7.59 (dd, J = 8.0, 2.0 Hz, 2H), 7.42 (d, J = 8.0 Hz, 2H), 7.18–7.07 (m, 2H), 3.10 (br, 3H), 1.52 (s, 18H); FAB-MS m/z calcd for $[\text{M}-(\text{CH}_3\text{CN})]^+$: 819.2, found 819.

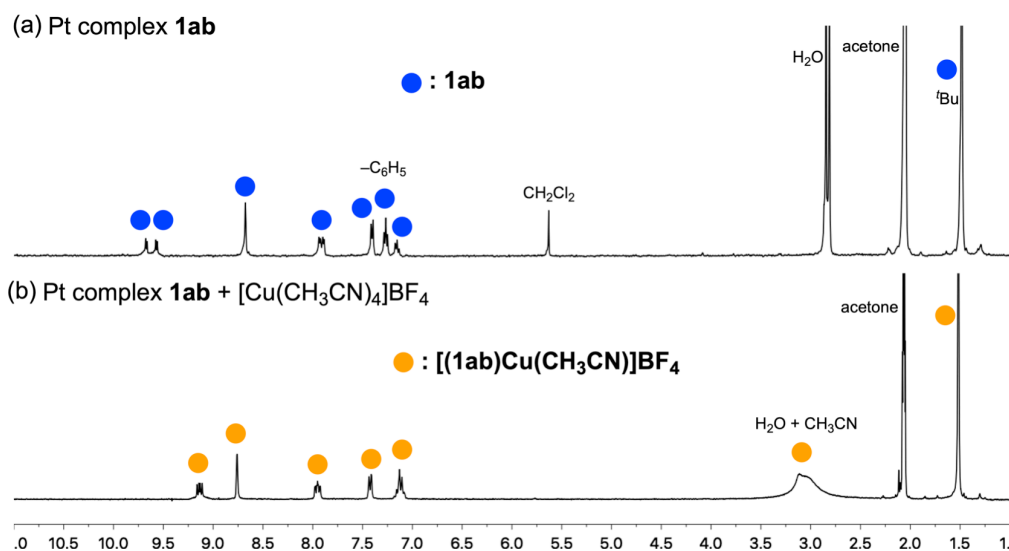


Fig. S5 ^1H NMR spectra (300 MHz, acetone- d_6 , r.t.) of Pt complex **1ab** (a) before and (b) after an addition of $[\text{Cu}(\text{CH}_3\text{CN})_4]\text{BF}_4$ in acetone- d_6 . The aromatic proton signals in the Pt complex unit were shifted, indicating that a formation of $[(\mathbf{1ab})\text{Cu}(\text{CH}_3\text{CN})]\text{BF}_4$ in solution.

X-ray crystallographic analysis

Crystals suitable for X-ray structural analyses were obtained by recrystallization from CH₂Cl₂/*n*-hexane ([**2**](BF₄)₃•7CH₂Cl₂) and CH₂Cl₂/*n*-hexane (**3**•2CH₂Cl₂), respectively. The crystal structures were initially solved by direct method (SHELXS-97). The positional and thermal parameters of non-H atoms were refined anisotropically by the full-matrix least-squares method except for disordering moieties. All calculations were performed using the CrystalStructure crystallographic software package³ except for refinement, which was performed using SHELXL-2014/7.

Table S1. Crystallographic data for [(**1ab**)₄Cu₃](BF₄)₃ (**[2]**(BF₄)₃) and [(**1ab**)₂Cu₄Br₄] (**3**).

	[2] (BF ₄) ₃ •7CH ₂ Cl ₂	3 •2CH ₂ Cl ₂
Empirical formula	C ₁₃₆ H ₁₁₆ B ₃ Cu ₃ F ₃₂ N ₈ Pt ₄ •7CH ₂ Cl ₂	C ₆₈ H ₅₈ Br ₄ Cu ₄ F ₁₀ N ₄ Pt ₂ •2CH ₂ Cl ₂
Formula weight	4068.37	2255.06
Temperature (K)	93	93
Wavelength (Å)	0.71075	0.71075
Crystal system	monoclinic	monoclinic
Space group	<i>P</i> 2 ₁ / <i>n</i> (#14)	<i>P</i> 2 ₁ / <i>n</i> (#14)
<i>a</i> (Å)	17.5253(16)	11.834(4)
<i>b</i> (Å)	34.487(3)	11.079(3)
<i>c</i> (Å)	25.961(2)	27.470(8)
α (deg)		
β (deg)	106.5884(13)	93.292(6)
γ (deg)		
<i>V</i> (Å ³)	15038(2)	3595.9(19)
<i>Z</i>	4	2
ρ_{calcd} (g/cm ³)	1.797	2.083
μ (Mo K α) (mm ⁻¹)	4.448	7.470
F(000)	7936	2160
Index ranges	-24 ≤ <i>h</i> ≤ 24 -47 ≤ <i>k</i> ≤ 47 -35 ≤ <i>l</i> ≤ 35	-16 ≤ <i>h</i> ≤ 16 -15 ≤ <i>k</i> ≤ 15 -37 ≤ <i>l</i> ≤ 33
Reflections collected	146936	38502
Independent reflections	40041 [<i>R</i> _{int} = 0.0613]	9594 [<i>R</i> _{int} = 0.0562]
Data / restraints / parameters	40041 / 0 / 1864	9594 / 12 / 442
Goodness-of-fit on <i>F</i> ²	1.074	1.163
Final <i>R</i> index [<i>I</i> > 2 σ (<i>I</i>)] ^a	<i>R</i> ₁ = 0.0504	<i>R</i> ₁ = 0.0556
<i>R</i> indices (all data) ^{a,b}	<i>R</i> ₁ = 0.0665, <i>wR</i> ₂ = 0.1513	<i>R</i> ₁ = 0.0673, <i>wR</i> ₂ = 0.1393
Largest diff. peak and hole (eÅ ⁻³)	-3.55 and 2.43	-2.88 and 2.93
CCDC number	2125697	2125698

^a $R_1 = \Sigma||F_o| - |F_c||/\Sigma|F_o|$. ^b $wR_2 = [\Sigma w(F_o^2 - F_c^2)^2]/\Sigma[w(F_o^2)^2]]^{1/2}$.

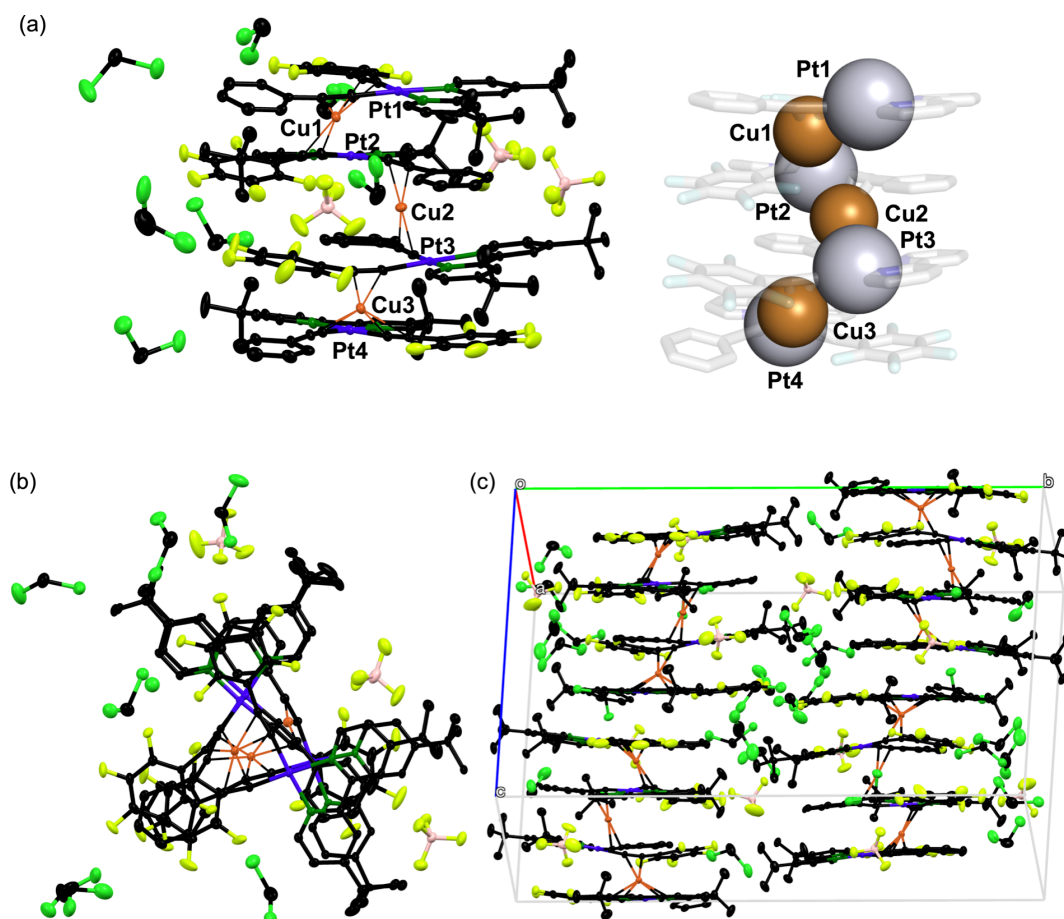


Fig. S6 ORTEP drawing (50% probability ellipsoids) of $[2](BF_4)_3 \cdot 7CH_2Cl_2$: (a) side view, (b) top view, and (c) crystal packing of the complex. Hydrogen atoms are omitted for clarity. This crystal structure contains both right- and left-handed helical Pt–Cu–Pt–Cu–Pt–Cu–Pt alignments, indicating the formation of racemic mixture of chiral Pt_4Cu_3 complex.

Table S2. Selected interatomic distances (Å) of $[2](BF_4)_3$.

atom–atom	distance (Å)	atom–atom	distance (Å)
Pt1···Cu1	2.994(2)	Cu2···Pt3	2.987(1)
Cu1···Pt2	3.394(2)	Pt3···Cu3	3.372(1)
Pt2···Cu2	2.817(1)	Cu3···Pt4	2.963(2)

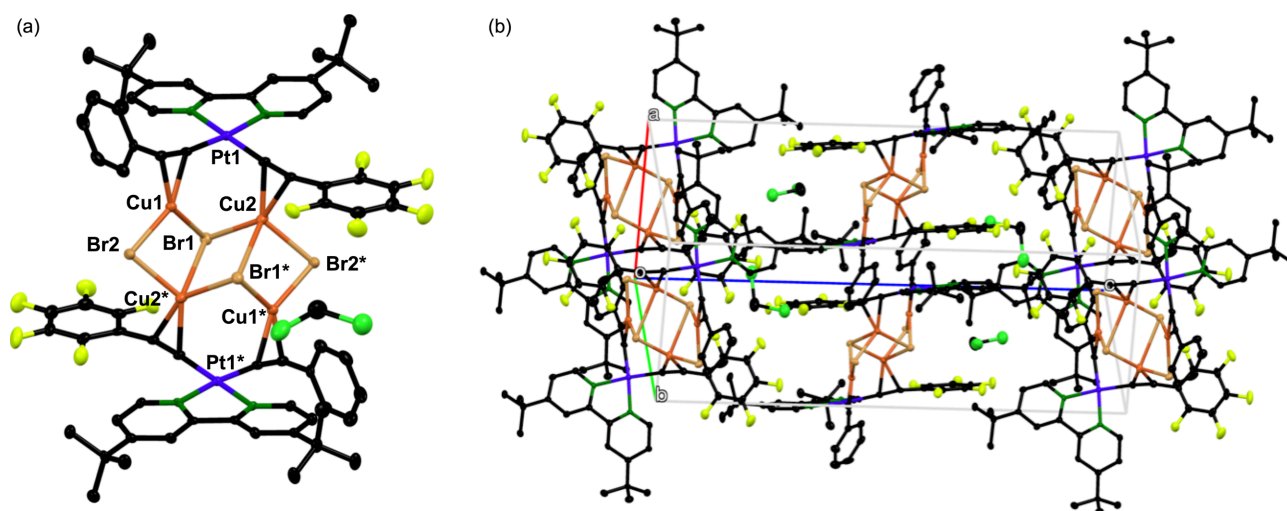


Fig. S7 (a) ORTEP drawing (50% probability ellipsoids) of $3 \cdot 2\text{CH}_2\text{Cl}_2$. (b) crystal packing of the complex. Hydrogen atoms are omitted for clarity. This $\text{Pt}_2\text{Cu}_4\text{Br}_4$ sandwich complex contains inversion center at the midpoint of $\text{Cu}2 \cdots \text{Cu}2^*$ and $\text{Br}1 \cdots \text{Br}1^*$ contact.

Table S3. Selected interatomic distances (Å) of **3**.

atom–atom	distance (Å)	atom–atom	distance (Å)
Pt1 \cdots Cu1	3.406(1)	Cu1–Br1	2.4318(12)
Pt1 \cdots Cu2	3.271(1)	Cu1–Br2	2.3848(11)
Cu1 \cdots Cu2	3.307(1)	Cu2–Br1*	2.4170(12)
		Cu2–Br2*	2.4363(12)

Photophysical properties

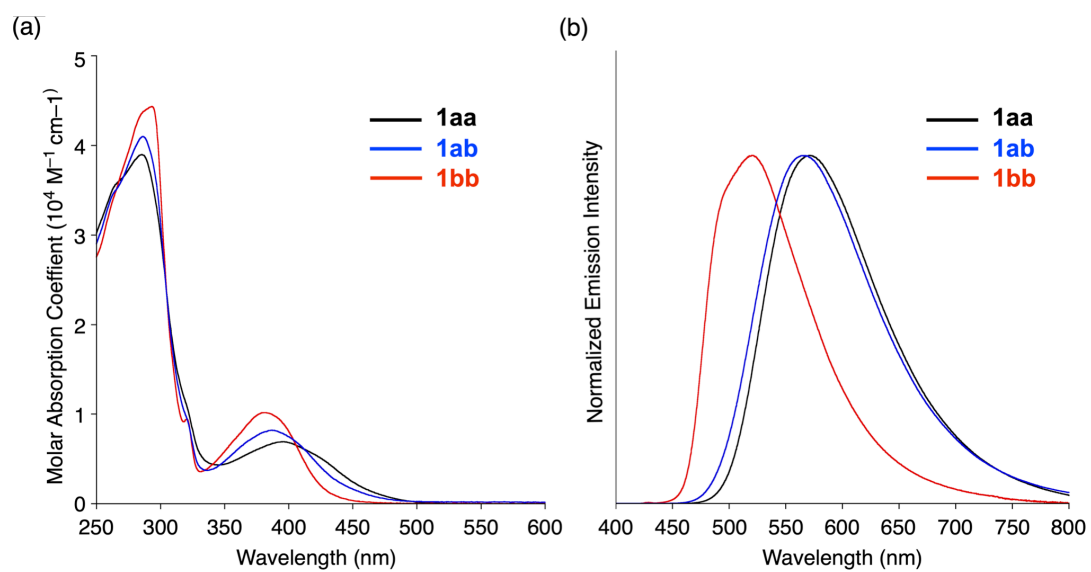


Fig. S8 (a) UV-Vis absorption spectra (CHCl_3 , r.t.) and (b) their normalized emission spectra (CHCl_3 , r.t., $\lambda_{\text{ex}} = 355 \text{ nm}$) of **1aa** (black), **1ab** (blue), and **1bb** (red).

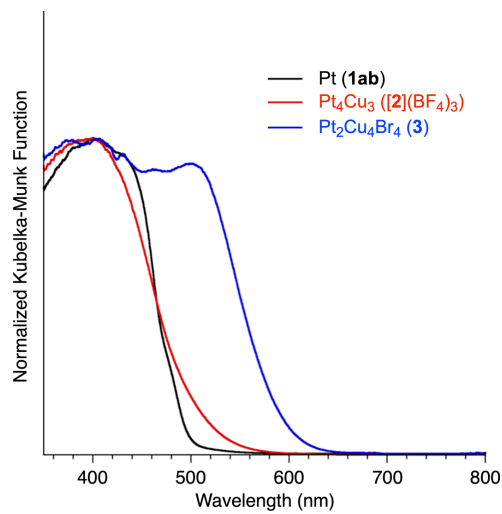


Fig. S9 UV-Vis diffuse reflectance spectra of **1ab**, **[2]**(BF_4)₃, and **3** in the solid state at 295 K.

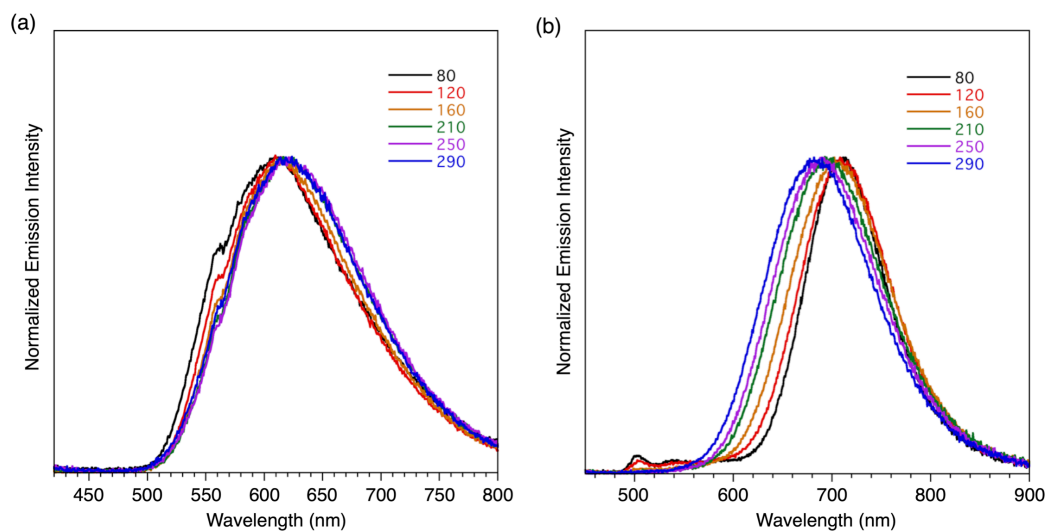


Fig. S10 Temperature-dependent emission spectra of (a) $[2](BF_4)_3$, and (b) **3** in the solid state. The emission spectra of **3** were gradually red-shifted upon decreasing the measurement temperature probably owing to shrinkage of the Cu_4Br_4 cluster unit.

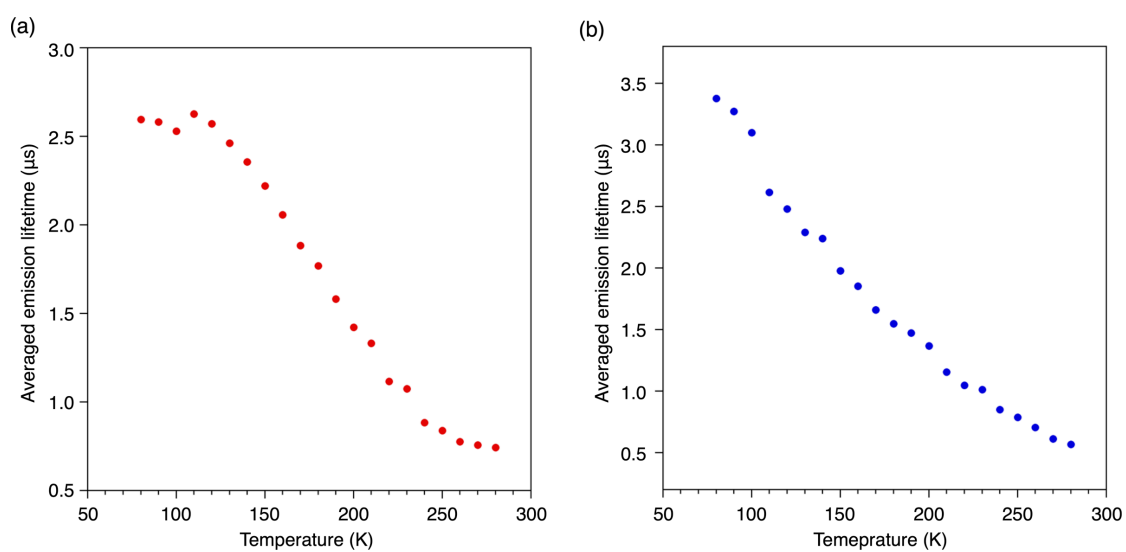


Fig. S11 Temperature-dependent emission lifetimes of (a) $[2](BF_4)_3$, and (b) **3** in the solid state.

Computational studies

Theoretical calculations for the complexes were conducted with Gaussian 16W (revision A.03).⁴ After optimizations of the ground-state geometries of the complexes were performed by using the B3LYP density functional theory (DFT), time-dependent (TD)-DFT calculations were then performed to estimate the energies and oscillator strengths f in the 5 lowest-energy singlet and 3 triplet absorption transitions with the CAM-B3LYP functional in order to improve accuracy for polarizability of long-range charge-transfer character of the excited states.⁵ In these calculations, for Pt atoms, basis sets with ECPs proposed by Christiansen et al were employed.⁶ For Cu and Br atoms, the LanL2DZ basis set was used to treat. For C, N, and H atoms, cc-pVDZ basis sets were applied. Crystallographic data were used as initial structures and the calculation of the complexes were carried out in a gas-phase. Owing to the large and flexible structure of $[2]^{3+}$, t Bu groups in $[2]^{3+}$ were replaced with Me groups at the bpy ligands. The Methyl derivative of $[2]^{3+}$ is denoted as $[2']^{3+}$ in the following tables. The metal atoms in $[2']^{3+}$ were managed as a rigid group and the position was fixed during the calculation. The structure of **1ab** was built up basis on the structure of **1aa**. Molecular orbitals with the isovalue of 0.04 were drawn by the GaussView 6.⁷ The Mayer bond index was estimated on the Multiwfn program.⁸

Table S4. Calculated singlet excited states of **1ab**.

Excited State	Transition	Energy (Wavelength)	Oscillator Strength
S ₁	MO148 → MO156 (20%)	2.8539 eV (434.44 nm)	0.0987
	MO155 → MO156 (80%)		
S ₂	MO147 → MO156 (20%)	3.2518 eV (381.28 nm)	0.2103
	MO154 → MO156 (80%)		
S ₃	MO151 → MO156	3.5513 eV (349.12 nm)	0.0023
S ₄	MO148 → MO157 (17%)	3.8052 eV (325.83 nm)	0.0142
	MO155 → MO157 (83%)		
S ₅	MO148 → MO158 (13%)	4.1624 eV (297.87 nm)	0.1300
	MO155 → MO157 (16%)		
	MO155 → MO158 (59%)		
	MO155 → MO161 (11%)		

MO155 : HOMO, MO156 : LUMO

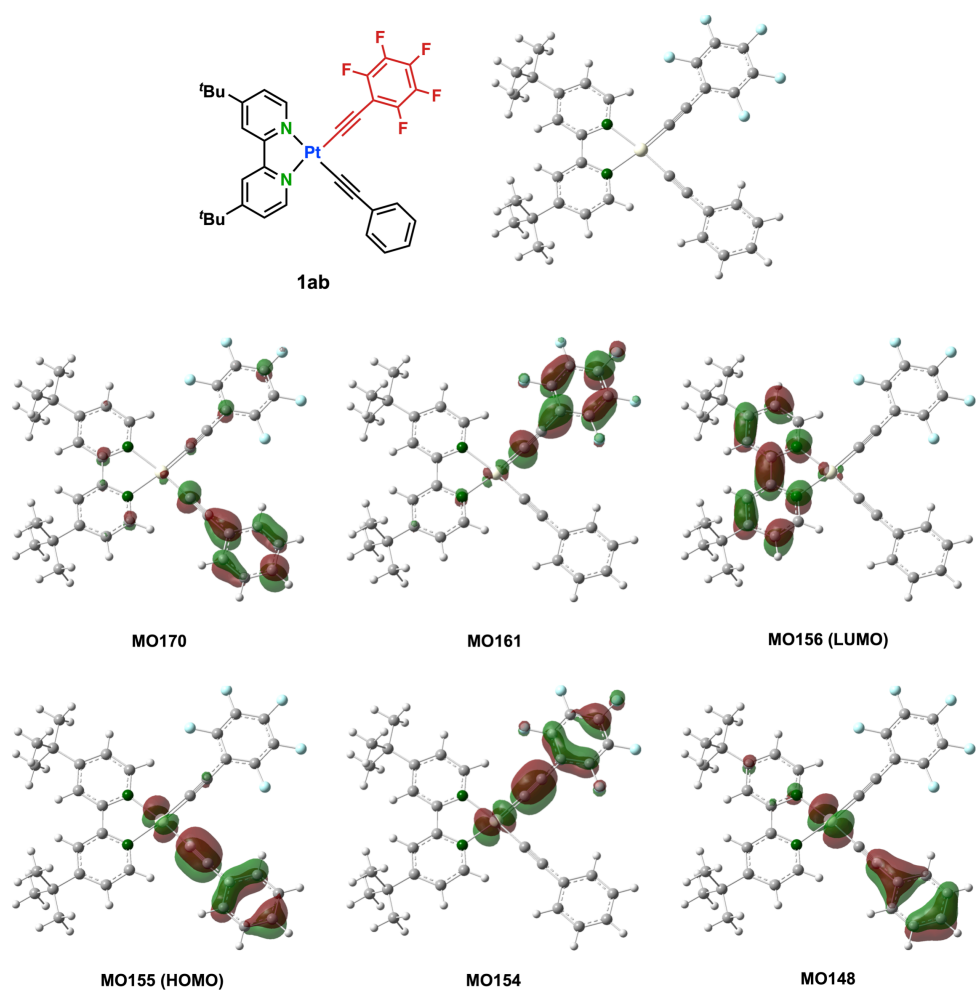


Fig. S12 Molecular orbitals of **1ab**.

Table S5. Calculated singlet excited states of the Me derivative of Pt₄Cu₃ complex cation [2']³⁺.

Excited State	Transition	Energy (Wavelength)	Oscillator Strength
S ₁	MO551 → MO554 (69%)	3.3768 eV (367.17 nm)	0.0797
	MO551 → MO555 (31%)		
S ₂	MO550 → MO555	3.4121 eV (363.37 nm)	0.1107
S ₃	MO545 → MO552 (12%)	3.4598 eV (358.36 nm)	0.0310
	MO547 → MO552 (17%)		
	MO550 → MO552 (71%)		
S ₄	MO550 → MO552 (17%)	3.4946 eV (354.79 nm)	0.0330
	MO551 → MO552 (38%)		
	MO551 → MO553 (45%)		
S ₅	MO544 → MO552 (10%)	3.5249 eV (351.74 nm)	0.0452
	MO549 → MO552 (31%)		
	MO549 → MO553 (48%)		
	MO550 → MO552 (11%)		

MO551 : HOMO, MO552 : LUMO

Table S6. Mayer bond order of the Me derivative of Pt₄Cu₃ complex cation [2']³⁺.

atom-atom	Bond order	atom-atom	distance (Å)
Pt1-Cu1	0.04	Pt3-Cu3	0.00
Cu1-Pt2	0.00	Cu3-Pt4	0.04
Pt2-Cu2	0.07		
Cu2-Pt3	0.10		

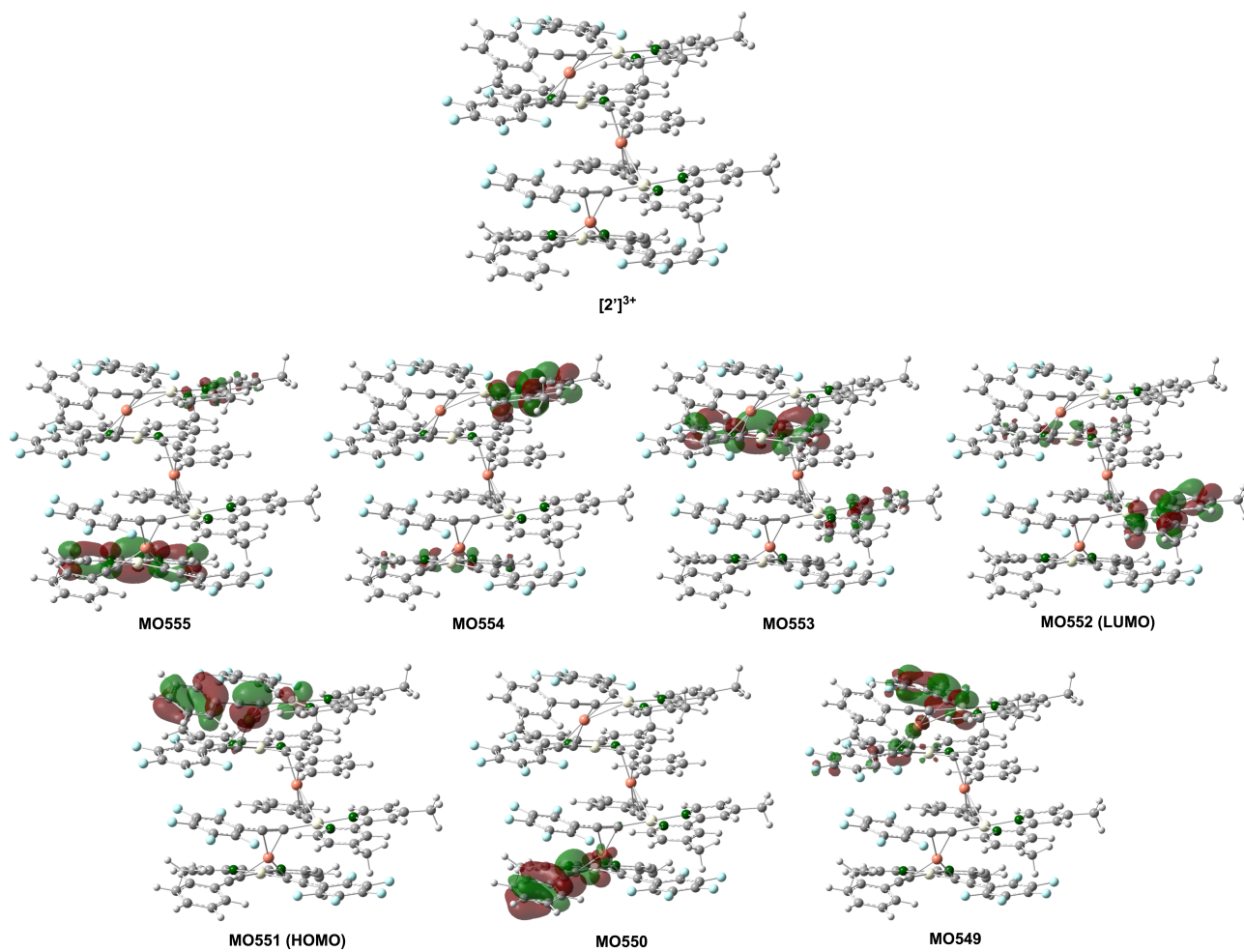


Fig. S13 Molecular orbitals of the Me derivative of Pt_4Cu_3 complex cation $[2']^{3+}$. Owing to the large and flexible structure of $[2]^{3+}$, tBu groups in $[2]^{3+}$ were replaced by Me groups at the bpy ligands.

Table S7. Calculated singlet excited states of **3**.

Excited State	Transition	Energy (Wavelength)	Oscillator Strength
S ₁	MO360 → MO364 (32%)	3.1193 eV (397.47 nm)	0.0022
	MO361 → MO363 (17%)		
	MO362 → MO363 (36%)		
	MO362 → MO364 (15%)		
S ₂	MO360 → MO363 (39%)	3.1310 eV (396.00 nm)	0.1248
	MO361 → MO364 (19%)		
	MO362 → MO364 (42%)		
S ₃	MO338 → MO364 (9%)	3.2275 eV (384.15 nm)	0.0472
	MO346 → MO364 (7%)		
	MO350 → MO364 (16%)		
	MO354 → MO363 (15%)		
	MO354 → MO364 (11%)		
	MO358 → MO363 (8%)		
	MO359 → MO364 (17%)		
	MO361 → MO364 (8%)		
MO362 → MO364 (9%)			
S ₄	MO338 → MO363 (11%)	3.2412 eV (382.53 nm)	0.0076
	MO350 → MO363 (18%)		
	MO354 → MO364 (16%)		
	MO355 → MO363 (8%)		
	MO357 → MO363 (11%)		
	MO358 → MO364 (9%)		
	MO359 → MO363 (18%)		
MO361 → MO363 (9%)			
S ₅	MO355 → MO363 (12%)	3.3117 eV (374.38 nm)	0.0016
	MO356 → MO363 (18%)		
	MO357 → MO364 (15%)		
	MO361 → MO363 (55%)		

MO362 : HOMO, MO363 : LUMO

Table S8. Mayer bond order of **3**.

atom–atom	Bond order	atom–atom	distance (Å)
Pt1–Cu1	0.02	Cu2–Br1	0.43
Pt1–Cu2	0.02	Cu2–Br1*	0.39
Cu1–Br1	0.43	Cu2–Br2*	0.48
Cu1–Br2	0.62		

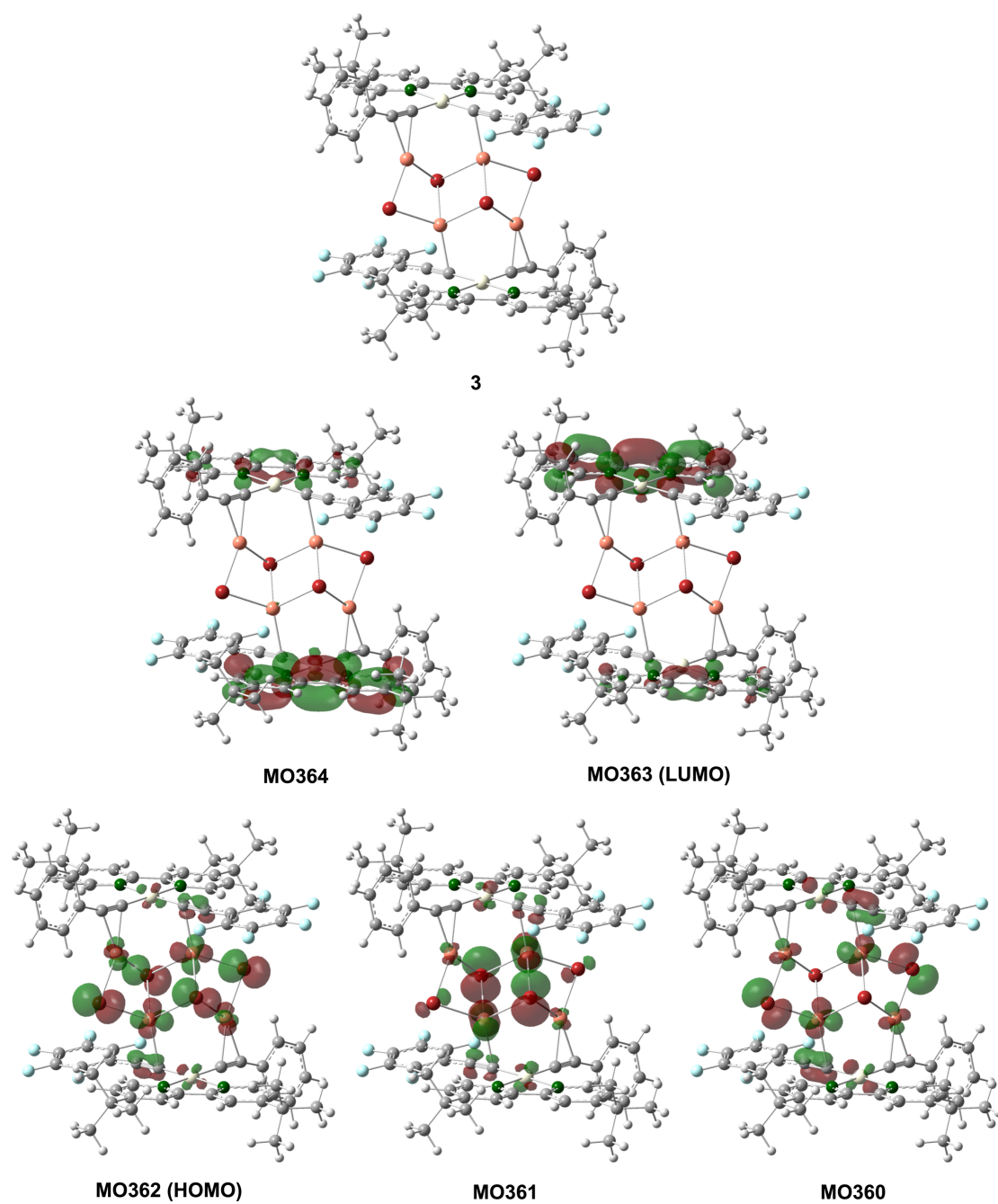


Fig. S14 Molecular orbitals of 3.

References

1. M. Hissler, W. B. Connick, D. K. Geiger, J. E. Mcgarrah, D. Lipa, R. J. Lachicotte, R. Eisenberg, *Inorg. Chem.* 2000, **39**, 447–457
2. W. Lu, M. C. W. Chan, N. Zhu, C.-M. Che, Z. He, and K.-Y. Wong, *Chem. Eur. J.* 2002, **9**, 6155–6166.
3. CrystalStructure 4.2: Crystal Structure Analysis Package, Rigaku Corporation, Tokyo, Japan, 2000–2017.
4. Gaussian 16, Revision A.03, M. J. Frisch, G. W. Trucks, H. B. Schlegel, G. E. Scuseria, M. A. Robb, J. R. Cheeseman, G. Scalmani, V. Barone, G. A. Petersson, H. Nakatsuji, X. Li, M. Caricato, A. V. Marenich, J. Bloino, B. G. Janesko, R. Gomperts, B. Mennucci, H. P. Hratchian, J. V. Ortiz, A. F. Izmaylov, J. L. Sonnenberg, D. Williams-Young, F. Ding, F. Lipparini, F. Egidi, J. Goings, B. Peng, A. Petrone, T. Henderson, D. Ranasinghe, V. G. Zakrzewski, J. Gao, N. Rega, G. Zheng, W. Liang, M. Hada, M. Ehara, K. Toyota, R. Fukuda, J. Hasegawa, M. Ishida, T. Nakajima, Y. Honda, O. Kitao, H. Nakai, T. Vreven, K. Throssell, J. A. Montgomery, Jr., J. E. Peralta, F. Ogliaro, M. J. Bearpark, J. J. Heyd, E. N. Brothers, K. N. Kudin, V. N. Staroverov, T. A. Keith, R. Kobayashi, J. Normand, K. Raghavachari, A. P. Rendell, J. C. Burant, S. S. Iyengar, J. Tomasi, M. Cossi, J. M. Millam, M. Klene, C. Adamo, R. Cammi, J. W. Ochterski, R. L. Martin, K. Morokuma, O. Farkas, J. B. Foresman, D. J. Fox, Gaussian, Inc., Wallingford CT, 2016.
5. T. Yanai, D. P. Tew, N. C. Handy, *Chem. Phys. Lett.* 2004, **393**, 51–57.
6. R. B. Ross, J. M. Powers, T. Atashroo, W. C. Ermler, L. A. LaJohn, P. A. Christiansen, *J. Chem. Phys.* 1990, **93**, 6654–6670.
7. GaussView, Version 5, R. Dennington, T. Keith J. Millam, Semichem Inc., Shawnee Mission, KS, 2009.
8. T. Lu, F. Chen, *J. Comput. Chem.*, 2012, **33**, 580–592.